Heliyon 10 (2024) e27436

Contents lists available at ScienceDirect

Heliyon

journal homepage: www.cell.com/heliyon

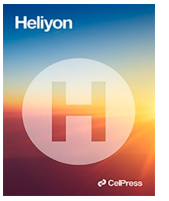

Research article

# Development and validation of a surgical planning tool for bone-conduction implants

Evan S. Simpson [a], Carlos D. Salgado [a], Seyed Alireza Rohani [b], Sumit K. Agrawal [a,b,c,d,1], Hanif M. Ladak [a,b,c,d,1,*]

[a] Department of Electrical and Computer Engineering, Western University, London, ON, Canada
[b] Department of Otolaryngology-Head and Neck Surgery, Western University, London, ON, Canada
[c] Department of Medical Biophysics, Western University, London, ON, Canada
[d] School of Biomedical Engineering, Western University, London, ON, Canada

ARTICLE INFO

*Keywords:*
Image analysis
BONEBRIDGE
Temporal bone
Surgical planning
Computed tomography
Bone conduction devices

ABSTRACT

*Background:* The BONEBRIDGE® (Med-El GmbH) is a bone-conduction device comprising an external audio processor and an internal Bone Conduction-Floating Mass Transducer (BC-FMT) surgically anchored to the temporal bone. Due to the implant's size, its placement may be challenging in certain anatomies, necessitating thorough surgical planning. Manual planning methods are laborious, time-intensive, and prone to errors. This study aimed to develop and validate an automated algorithm for determining skull thickness, aiding in the surgical planning of the BONEBRIDGE and other devices requiring similar bone thickness estimations.

*Materials and methods:* Twelve cadaveric temporal bones underwent clinical computed tomography (CT). A custom Python algorithm was developed to automatically segment bone from soft tissue, generate 3D models, and perform ray-tracing to estimate bone thickness. Two thickness colormaps were generated for each sample: the cortical thickness to the first air cell and the total thickness down to the dura. The algorithm was validated against expert manual measurements to achieve consensus interpretation.

*Results:* The algorithm estimated bone-to-air thicknesses (mean = 4.7 mm, 95% Confidence Interval [CI] of 4.3–5.0 mm) that closely matched the expert measurements (mean = 4.7 mm, CI of 4.4–5.0 mm), with a mean absolute difference (MAD) of 0.3 mm. Similarly, the algorithm's estimations to the dura (6.0 mm, CI of 5.4–6.5 mm) were comparable to the expert markings (5.9 mm, CI of 5.4–6.5 mm), with a MAD of 0.3 mm.

*Conclusions:* The first automated algorithm to calculate skull thickness to both the air cells and dura in the temporal bone was developed. Colormaps were optimized to aid with the surgical planning of BONEBRIDGE implantation, however the tool can be generalized to aid in the surgical planning of any bone thickness application. The tool was published as a freely available extension to the open-source 3D Slicer software program (www.slicer.org).

* Corresponding author. Department of Medical Biophysics Western University 1151 Richmond Street London, Ontario, N6A 3K7, Canada.
*E-mail address:* hladak@uwo.ca (H.M. Ladak).
[1] co-senior authors.

https://doi.org/10.1016/j.heliyon.2024.e27436
Received 17 May 2023; Received in revised form 21 February 2024; Accepted 28 February 2024
Available online 5 March 2024

## 1. Background

The BONEBRIDGE® by Med-El GmbH (Innsbruck, Austria) is a bone-conduction implant (BCI) used to address conductive or mixed mild-to-moderate hearing loss in patients who do not achieve sufficient improvement with conventional hearing aids [1]. It comprises an externally worn audio processor and a subcutaneous Bone Conduction-Floating Mass Transducer (BC-FMT) that is surgically anchored to the temporal bone [1]. The device is categorized as a semi-implantable, transcutaneous BCI because the external component powers the BC-FMT [2]. The device's active nature enables it to bypass the sound transmission dampening effects of the skin, thereby overcoming the limitations of passive bone conduction devices [3,4]. Fig. 1 illustrates an implanted BONEBRIDGE.

The BONEBRIDGE was first introduced in Europe in September 2012 [5]. The first North American implantation occurred in April 2013 at the London Health Sciences Centre (LHSC) in London, Ontario, Canada [6]. In Canada, the BONEBRIDGE is approved for use in all patients over five years old with conductive or mixed hearing loss and bone conduction thresholds of $\leq$45 dB measured at 0.5–3.0 kHz. It is also suitable for patients with single-sided deafness, where the contralateral ear has a hearing threshold between 0 and 20 dB measured at 0.5–3.0 kHz [6]. For patients with symmetric conductive or mixed hearing loss, a bilateral fitting may be considered. In July 2018, the BONEBRIDGE received "De Novo clearance" from the United States (US) Food and Drug Administration (FDA) [7]. The current indications are the same as mentioned above, except that the US indication for implantation is currently for patients over 12 years old.

One drawback of the BONEBRIDGE (BCI 601) is its relatively large BC-FMT, measuring 8.7 mm in height and 15.8 mm in diameter. The latest generation, BONEBRIDGE (BCI 602), addresses this by reducing the BC-FMT depth to 4.5 mm by increasing its diameter to 18.2 mm, and relocating some components above the bony surface [8]. Despite these improvements, thorough pre-surgical planning is essential to identify a safe, spacious location for the implant. Common implantation sites for the BONEBRIDGE include the mastoid, retrosigmoid, and middle fossa regions, each with its own advantages and disadvantages [6,9–11]. The mastoid approach, may be challenging due to limited space between the sigmoid sinus, tegmen mastoideum, external auditory canal, and facial nerve. This location is excluded in patients with chronic otitis media or prior mastoidectomies [4]. In such cases, the retrosigmoid and middle fossa regions are viable alternatives, though skull thickness may hinder complete implantation without dural compression or the use of BCI lifts [5,6,12–14]. Additionally, the screws used to secure the implant typically require 3–4 mm of cortical bone thickness for fixation, which can be problematic in highly pneumatized temporal bones where the cortex near the air cells may be very thin.

Current surgical planning methods for various BCIs involve using computed tomography (CT) images to manually measure thickness [15]. Since these measurements are usually taken on two-dimensional (2D) slices, transferring them to the operating room can be challenging. Previous studies have explored tools for visualizing the BC-FMT in CT slices and creating three-dimensional (3D) reconstructions. However, these methods are time-consuming, expensive, and require extensive manual image manipulation [6,13,16–19]. Additionally, many of these approaches do not account for air cells in thickness estimates.

The main goal of this study was to create a 3D, open-source, automated algorithm for estimating thickness to aid in surgical planning for the BONEBRIDGE. This innovative technique provides comprehensive measurements of bone thickness, including consideration of air cells. A secondary aim was to compare the algorithm with manual expert measurements, which are currently the standard practice in surgery. This novel algorithm is expected to enhance the clinical workflow for pre-surgical planning not only for the BONEBRIDGE BCI but also for other bone-anchored devices.

## 2. Materials and methods

### 2.1. Clinical CT images

Twelve cadaveric temporal bones were imaged using a Discovery CT750 HD Clinical Scanner (GE Healthcare, Chicago, IL). The scanner settings included a resolution of 234 μm, a slice thickness of 0.625 mm, and an x-ray voltage of 120 kV.

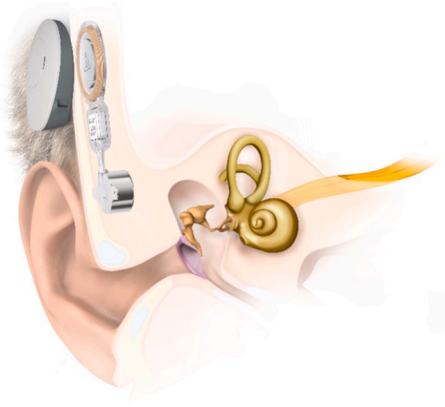

**Fig. 1.** Cross-section of an implanted BONEBRIDGE bone-conduction device. Image courtesy of the device manufacturer.

Ethics approval for this study was granted by Western University's Committee for Cadaveric Use in Research (approval number #19062014).

### 2.2. Algorithm development

#### 2.2.1. 3D slicer module

A custom scripted module was developed for the open-source software 3D Slicer (www.slicer.org) to provide the algorithm with a suitable user-interface and ease-of-use for the end user. The module was written in Python and can directly access ITK (https://itk.org) and VTK (https://vtk.org) packages, and 3D Slicer image software toolkits. Any user may download the module and import it into 3D Slicer. The module's user-interface contains several configuration options, a one-click execute function, and algorithm progress status text.

The following sections describe the sequential steps of the algorithm as implemented in the module. As an overview, first bone is segmented from all other structures. Ray casting is then applied twice: first to generate a polygonal mesh on the outer surface of the bone, and second to estimate the bone thickness and distance to air cells. Then, the thickness and distance values are visualized using a colormap.

#### 2.2.2. Segmentation

Images imported into the module are first processed with a thresholding image segmentation filter to separate the bone from surrounding soft tissue. Otsu's method [20] in 3D slicer is then used to perform automatic image thresholding to remove the dura and excess material. A morphological opening smoothing filter is applied to reduce noise artifacts generated during the initial segmentation. Next, a keep-largest island-removal filter is applied to the segmentation to ensure that the resultant segmentation contains one closed-surface bone volume. Lastly, the resulting image segmentation is converted into a model to ensure image spacing, origin, and dimensions are applied to future calculations.

#### 2.2.3. Ray-casting

Segmented models are processed with a two-step ray casting procedure, adopted from an algorithm developed by Albani et al. [21]. First, a 2D grid of rays is casted downward toward the bone's outer surface. The points of intersection are used to create a polygon surface mesh that represents the top surface of the bone. The spacing between grid lines can be controlled to alter the number of polygons that will be used to form the surface mesh. This is represented within the module as a render-quality setting and provides support for low-end to high-end graphics machines. Second, rays are casted through the center of each surface-mesh polygon along its normal vector and toward the inside of the skull. Points of intersection are recorded and contain the entry and exit points of the ray through the bone and any present air cells. The ray-casting algorithm is depicted in Fig. 2.

#### 2.2.4. Visualization

Two sets of thickness estimates were generated for each sample: the first indicating the thickness from the outer surface to the first air cell, and the second indicating the distance from the outer surface to the dura. In this study, colormaps representing these estimates were overlaid onto the segmented models. The colormap for the distance to the first air cell was set from 0 to 4 mm, reflecting the cortical thickness required to fully embed the screws of the BC-FMT. The default colormap for the distance to the dura was set from 0 to 8.7 mm, corresponding to the thickness of the actual BC-FMT in the BCI 601. These ranges can be easily adjusted based on the specific application or implant.

### 2.3. Validation

To compare the algorithm's estimations with expert observations, measurements were conducted by a neurotologist experienced in BONEBRIDGE implantation (S.K.A.) and an image processing student (C.S.) using a set of uniformly distributed points (n = 200) placed on the cortical layer of the temporal bone. Some of these points are illustrated in Fig. 3A. These points were strategically distributed to cover the most common implantation areas in the mastoid, retrosigmoid, and middle fossa regions. The expert visualized each point in the axial slice view and placed fiducials on the cortical bone, first air cell, and dura, as demonstrated in Fig. 3B. After achieving a

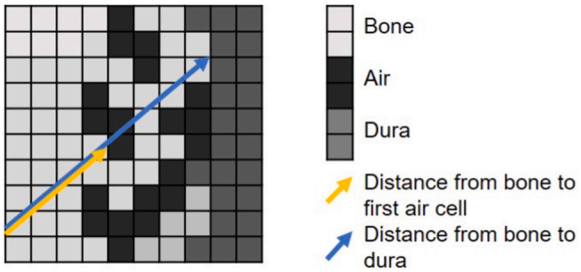


**Fig. 2.** Schematic illustrating the ray-casting algorithm to the first air cell and to dura.

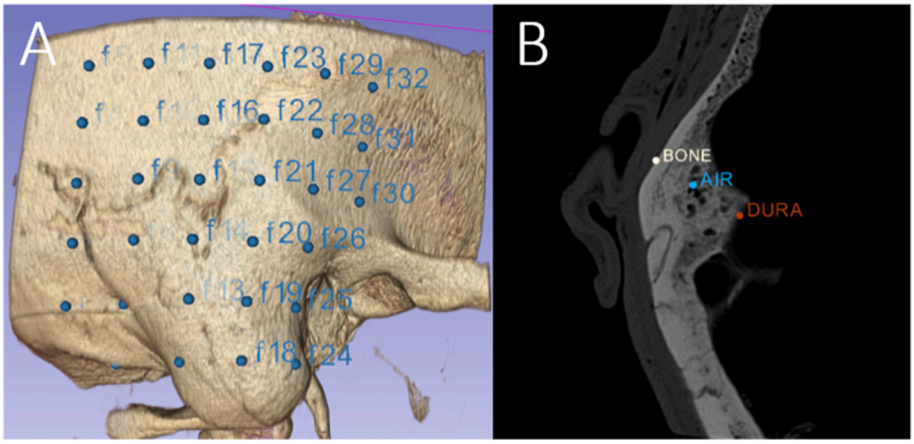


**Fig. 3.** Grid of evenly distributed points laid by the program (A). Expert measurements from the cortical bone in reference to the first air cell and to dura (B).

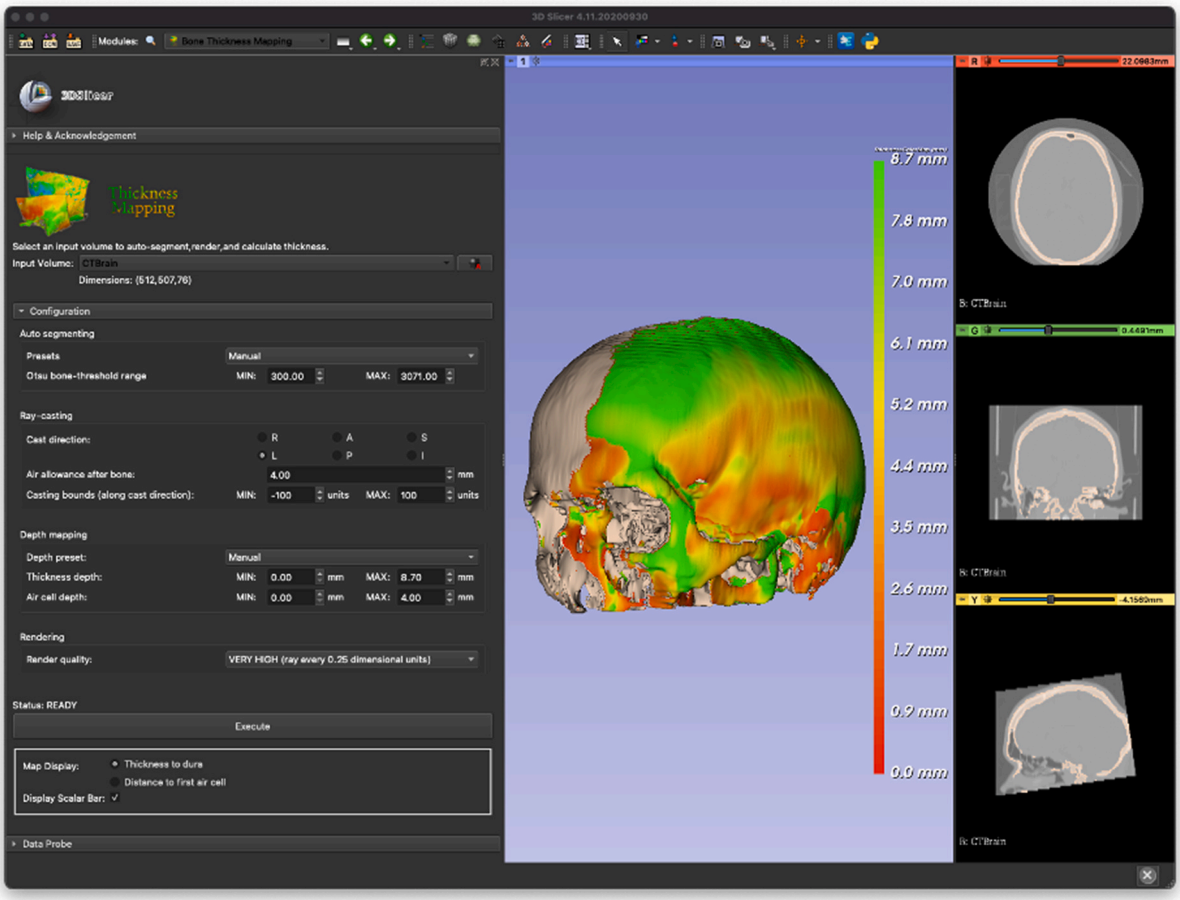


**Fig. 4.** User-interface of Bone Thickness Mapping module within the 3D Slicer application.

consensus interpretation, the fiducials were converted to millimeters to correspond to the distances calculated by the algorithm.

### 2.4. Statistical analyses

The data analysis was performed using IBM SPSS Statistics (Version 23.0, IBM Corp., Armonk, New York, USA) and the graphs were created using GraphPad Prism (Version 7.00, GraphPad Software, La Jolla, California, USA). The analysis included calculating the means, 95% confidence intervals (95% CI), differences, and mean absolute differences (MAD). Normality was assessed using skewness, kurtosis, and the Shapiro-Wilk test. The Spearman's rank correlation coefficient was computed, and differences between the algorithm and expert measurements were assessed using the Wilcoxon signed-rank test. Significance was set at $p < 0.05$, and multiple comparisons were adjusted using the Holm-Bonferroni method. The differences and absolute differences between the algorithm and expert observations were then determined.

## 3. Results

### 3.1. Algorithm

The ray-casting algorithm was effectively implemented, leading to the development of a surgical planning module for 3D Slicer intended for pre-operative use by surgeons. Fig. 4 displays the user interface of the module within 3D Slicer. Each cortical surface was composed of roughly 140,000 quadrilaterals, and the program was designed to be multi-threaded, enabling the simultaneous processing of multiple samples. The workstation utilized in this study was equipped with a core-i7 processor (Intel Corporation, Santa Clara, CA, USA), 24 GB of memory, and an Nvidia GTX 970 graphics card (Nvidia Corporation, Santa Clara, CA, USA). On average, the total computation time per sample was about 4 min.

Fig. 5 displays thickness estimation colormaps generated by the algorithm, showing measurements from the cortical bone to the first air cells (Fig. 5A and C) and from the bone to the dura (Fig. 5B and D) for two samples: one with thick cortical bone (Fig. 5A and B) and one with thin cortical bone (Fig. 5C and D). In the sample with thick bone, the colormap indicates that most areas, except for the most anterior part of the middle fossa, could accommodate implant screws of up to 6 mm in length (4 mm bone penetration), as well as the BC-FMT, while avoiding the most inferior part of the mastoid. In areas with thinner bone, successful implantation would require dural compression and/or BCI lifts. The colormap for the thinner bone sample reveals the sigmoid sinus in the bone-to-dura thickness map, suggesting that the most suitable location for the BC-FMT and screws would be in the medial mastoid. Artifacts are noticeable along the zygomatic root due to its composition as a tube of bone surrounded by air. Therefore, it is important to note that the tool is intended to complement, rather than replace, clinical decision-making. Surgeons should confirm all potential implantation areas suggested by the tool before proceeding with implantation.

### 3.2. Validation

#### 3.2.1. Bone to air cell measurements

When comparing all points ($n = 200$), the automated bone-to-air thickness measurements (mean = 4.7 mm, CI of 4.3–5.0 mm) and expert measurements (mean = 4.7 mm, CI of 4.4–5.0 mm) did not show a significant difference, with a p-value of 0.36. The MAD was small (0.3 mm, CI of 0.26–0.34 mm), which is approximately the size of a voxel on a clinical CT scan. Fig. 6 illustrates the raw data, demonstrating a strong correlation between the algorithm and expert measurements ($r = 0.98$, $p < 0.001$).

An analysis of implantation sub-regions (mastoid, retrosigmoid, or middle fossa) is depicted in Fig. 7. In the mastoid area ($n = 17$), there was no significant difference between the automated (mean = 4.4 mm, CI of 3.2–5.7 mm) and expert (mean = 4.5 mm, CI of 3.2–5.8 mm) measurements ($p = 0.98$). Similarly, in the middle fossa ($n = 140$), there was no significant difference between the automated (mean = 4.3 mm, CI of 3.9–4.7 mm) and expert (mean = 4.3 mm, CI of 4.0–4.7 mm) thicknesses ($p = 0.76$). However, in the retrosigmoid area ($n = 23$), the automated thickness measurements (mean = 5.6 mm, CI of 4.5–6.6 mm) were slightly smaller than the expert markings (mean = 5.8 mm, CI of 4.9–6.7 mm; $Z = -2.1$, $p = 0.03$), although this difference was not significant when controlling

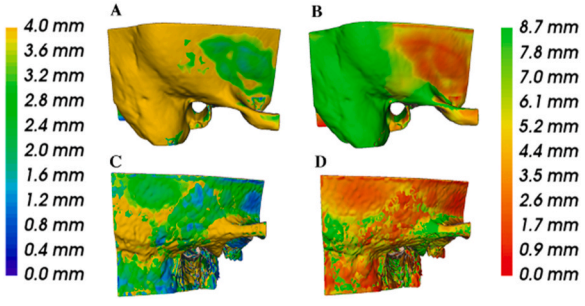


**Fig. 5.** Thickness colormap from bone-to-air cell (LEFT) and bone-to-dura (RIGHT). Sample with thick cortical bone (TOP). Sample with thinner cortical bone (BOTTOM). Units in mm.

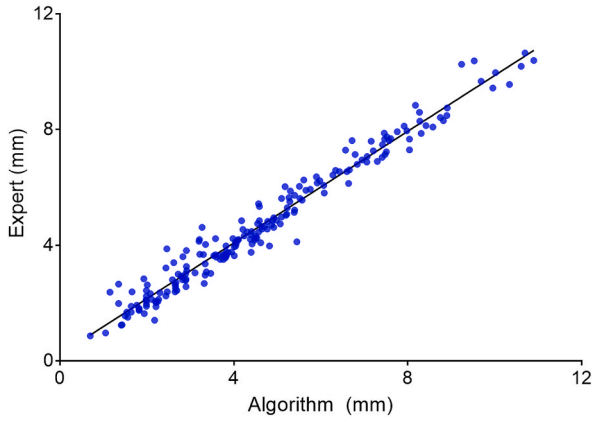


**Fig. 6.** Scatter-plot of measurements from bone to air cell by the algorithm and expert.

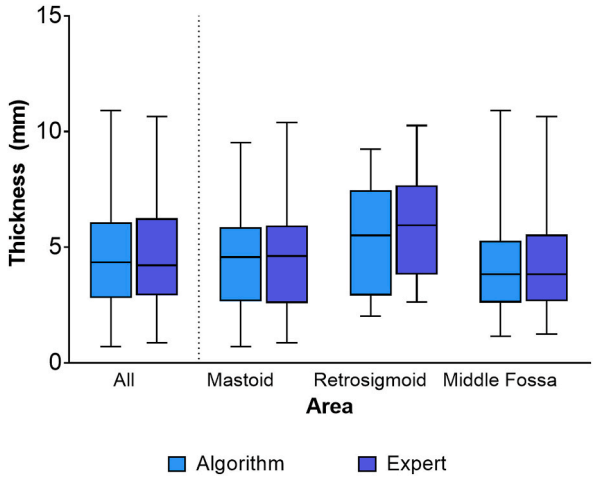


**Fig. 7.** Box-plot of algorithm and expert measurements to the first air cell. All points, mastoid, middle fossa, and retrosigmoid areas.

for family-wise error using the Holm-Bonferroni method.

### *3.2.2. Bone to dura measurements*

When comparing all points (n = 200), the automated bone-to-dura thickness measurements (mean = 6.0 mm, CI of 5.4–6.5 mm)

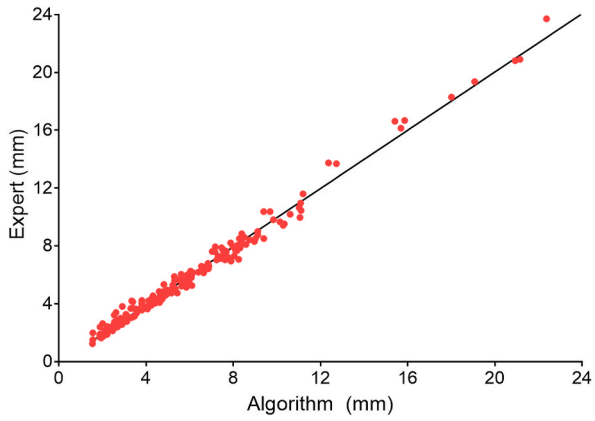


**Fig. 8.** Scatter-plot of measurements from bone to dura by the algorithm and expert.

and expert measurements (mean = 5.9 mm, CI of 5.4–6.5 mm) were found to be significantly different ($Z = -3.7$, $p < 0.01$). The MAD was small (0.3 mm, CI of 0.28–0.35 mm). Fig. 8 illustrates the raw data, indicating a strong correlation between the algorithm and expert measurements ($r = 0.99$, $p < 0.001$).

Sub-region results are presented in Fig. 9. In the mastoid (n = 17), there was no significant difference between the automated (mean = 14.5 mm, CI of 11.2–17.7 mm) and expert (mean = 14.8 mm, CI of 11.5–18.2 mm) measurements ($p = 0.06$). Similarly, in the retrosigmoid area (n = 23), the automated (mean = 6.1 mm, CI of 5.1–7.1 mm) and expert (mean = 6.3 mm, CI of 5.4–7.2 mm) measurements did not show a significant difference ($p = 0.16$). However, in the middle fossa (n = 140), the automated bone-to-dura thickness measurements (mean = 4.8 mm, CI of 4.4–5.2 mm) were significantly different from the expert markings (mean = 4.6 mm, CI of 4.3–5.0 mm; $Z = -5.8$, $p < 0.01$).

Fig. 10 illustrates the differences between the expert and algorithm for bone-to-air cell and bone-to-dura measurements. For bone-to-air measurements, the MAD values by sub-region were 0.4 mm (CI of 0.14–0.60 mm) for the mastoid, 0.3 mm (CI of 0.23–0.32 mm) for the middle fossa, and 0.5 mm (CI of 0.31–0.60 mm) for the retrosigmoid. The MAD for dura measurements were 0.6 mm (CI of 0.40–0.80 mm) for the mastoid, 0.3 mm (CI of 0.23–0.30 mm) for the middle fossa, and 0.5 mm (CI of 0.35–0.60 mm) for the retrosigmoid.

Table 1 provides an overview of the variance within the populations, displaying the algorithm, expert, and MAD means along with their respective 95% CIs.

## 4. Discussion

The BONEBRIDGE has been effectively used to address mild-to-moderate hearing loss in patients with conductive or mixed hearing loss, resulting in functional improvements and high user satisfaction [10]. However, the surgical placement of the BONEBRIDGE poses challenges due to the need to find a thick enough portion of the temporal bone to accommodate the large implantable BC-FMT. The most common approach to surgical planning, as reported in the literature, involves manual image-guided placement using CT images. This approach entails visualizing an implant model in CT regions corresponding to potential placement locations, without providing thickness maps.

Previous efforts have sought to enhance the surgical planning process of the BONEBRIDGE through 3D visualization techniques. Many groups have utilized the freely available tool BB FASTVIEW (Center for Technical Studies and Research at the University of Navarra, Spain) for visualizing the BC-FMT within CT slices and 3D reconstructions [6,13,16]. However, the use of this tool has been described as time-consuming, with the navigation process taking over 90 min. Plontke et al. [17] utilized the commercial visualization software Amira (Thermo Fisher Scientific, Waltham, MA, USA) to simulate the implant inside 3D images, but this tool is expensive, not readily accessible to surgeons, and requires manual determination of the optimal implant location [17].

Todt et al. developed [22] and reviewed [23] a simulator for the BONEBRIDGE using the open-source software ZIBAmira (Zuse Institute Berlin, Germany). However, their approach, which involved statistical shape modeling for segmentation, has limitations (e.g., requiring large datasets) that make it unsuitable for thickness estimation [23]. Law et al. [24] used the program 3D Slicer to visualize the BC-FMT and screws for finding a suitable implantation location by measuring bone thickness at skull landmarks. Matsumoto et al. [25] developed a surface template-assisted marker positioning (STAMP) method for performing image-guided surgery, later adapting the method for the BONEBRIDGE (BB-STAMP) [26]. However, the BB-STAMP method is costly and therefore impractical for many centers [26]. Among these studies, Law and colleagues [24] did not consider perforating large air cells, whereas most other studies considered air cells as part of the bone in their manual estimations. In contrast, Inui et al. [27] presented ray casting as a general application to determine thickness and clearance in 3D objects.

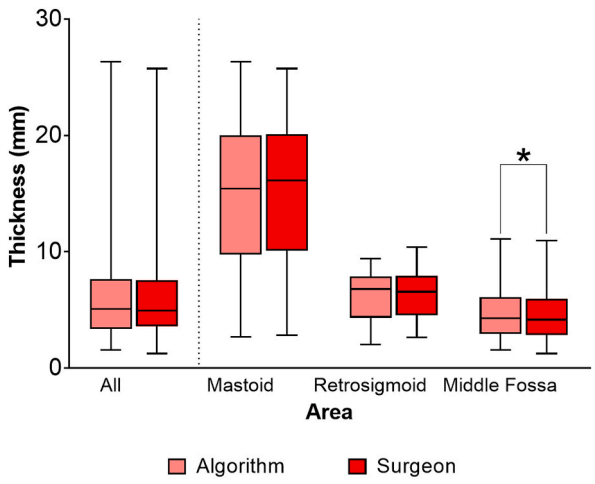


**Fig. 9.** Box-plot of algorithm and expert measurements to the dura. All points, mastoid, middle fossa, and retrosigmoid areas. The asterisk represents significant difference, $p < 0.05$.

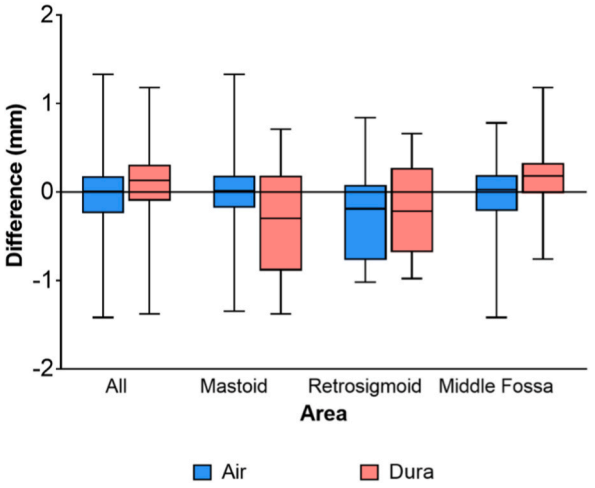


**Fig. 10.** Box-plot of algorithm and expert differences in millimeters. Positive results indicate the algorithm had a larger estimate than the expert. Negative results indicate larger measurements by the expert.

**Table 1**
Mean absolute difference (MAD) results by region with 95% confidence intervals. Measurements in millimeters (mm)

| Thickness to Air Cells | | | | | | |
|---|---|---|---|---|---|---|
| Area | Algorithm | | Expert | | MAD | |
| | Mean | 95% CI | Mean | 95% CI | Mean | 95% CI |
| Mastoid[a] | 4.4 | 3.2–5.7 | 4.5 | 3.2–5.8 | 0.4 | 0.14–0.60 |
| Middle Fossa[b] | 4.3 | 3.9–4.7 | 4.3 | 4.0–4.7 | 0.3 | 0.23–0.32 |
| Retrosigmoid[c] | 5.6 | 4.5–6.6 | 5.8 | 4.9–6.7 | 0.5 | 0.31–0.60 |
| All[d] | 4.7 | 4.3–5.0 | 4.7 | 4.4–5.0 | 0.3 | 0.26–0.34 |
| **Thickness to Dura** | | | | | | |
| **Area** | **Algorithm** | | **Expert** | | **MAD** | |
| | **Mean** | **95% CI** | **Mean** | **95% CI** | **Mean** | **95% CI** |
| Mastoid[a] | 14.5 | 11.2–17.7 | 14.8 | 11.5–18.2 | 0.6 | 0.40–0.80 |
| Middle Fossa[b] | 4.8 | 4.4–5.2 | 4.6 | 4.3–5.0 | 0.3 | 0.23–0.30 |
| Retrosigmoid[c] | 6.1 | 5.1–7.1 | 6.3 | 5.4–7.2 | 0.5 | 0.35–0.60 |
| All[d] | 6.0 | 5.4–6.5 | 5.9 | 5.4–6.5 | 0.3 | 0.28–0.35 |

[a] n = 17.
[b] n = 140.
[c] n = 23.
[d] n = 200, including 20 points close to implantation sites.

Wimmer et al. [18] described a technique using Amira software to measure temporal bone thickness for surgical planning of BCIs. This method involved thresholding, cropping, manual editing, and morphological filtering to find the inner and outer bone surfaces. Thickness was estimated by calculating the Euclidean distance between vertices, generating a distance from the cortical bone to the dura mater. However, air cells were not considered, as they had been filled via a morphological hole filter. The final iteration of this technique, described by Barakchieva et al. [19], was developed using the C++ programming language.

In this study, a thickness estimation algorithm was developed that accounted for air cells in the temporal bone, thus preventing overestimation of thicknesses to air and to the dura mater. The algorithm's running time per bone was approximately 4 min. Comparison with manual expert measurements revealed excellent correlation.

Measurements to the dura showed statistically significant variation ($p < 0.01$). Nevertheless, the mean overall MAD was 0.3 mm (CI of 0.28–0.35 mm), with region-specific MADs of 0.6 mm for the mastoid, 0.3 mm for the middle fossa, and 0.5 mm for the retrosigmoid. These differences were below the 0.625 mm axial slice thickness, indicating that the variance magnitude was not clinically significant. The MAD between air measurements was also below the image resolution, at 0.3 mm for all (n = 200) measurements. Surgeons can adjust for thickness variances of ±1 mm intraoperatively due to the availability of various lifts and dural compression methods. Our results suggest that with the current parameters, this algorithm can assist in the surgical planning of the BONEBRIDGE in all three currently used implantation areas (mastoid, retrosigmoid, and middle fossa).

In most areas, the difference between algorithm and manual thickness measurements is generally small because the difference in angle between the direction of manual measurement and the direction of the ray cast by the algorithm is also small. Despite the small differences between manual and automatic measurements, the algorithm offers the advantage of computing thickness at many points

automatically, enabling a colour-coded thickness map to be overlaid on the temporal bone. This map facilitates a very quick visual scan of the bone to determine areas where the bone is the thickest. By contrast, manual measurements at the numerous points needed to generate an accurate thickness map would be time consuming and labour intensive.

However, certain measurements obtained through the algorithm showed significant discrepancies compared to those taken by the expert surgeon. These outliers were likely a result of the algorithm's calculation of normal directions using the triangles from the outer cortical surface in 3D. In contrast, the surgeon conducted thickness measurements solely using the axial orientation, which is the standard practice for analyzing head CT scans but represents 2D data. These outliers were omitted from the statistical analyses. The measurements included in the analyses thus demonstrated comparable thickness measurements between the program and the surgeon while ensuring a large sample size for statistical power.

Most bone-anchored medical devices require specific placement, similar to the BONEBRIDGE device. 3D Slicer was specifically chosen in this study as the software implementation platform as it is free to use, open-source, well documented, and backed by an active community of users and developers. This will allow our algorithm's applications to extend to a wide variety of medical disciplines such as orthopedics and dentistry, in addition to other implantable devices in the field of Head and Neck Surgery. The module was published to 3D Slicer, available within its Extension Manager index as a one-click install package under the title "Bone Thickness Mapping". Additionally, the module's source code is hosted as a public repository on the open-source collaboration platform GitHub, under the title "SlicerBoneThicknessMappingExtension" [28].

Future work could include the use of deep learning algorithms to automatically extract the skull and segment associated structures [29], however the current module was developed with minimal hardware requirements (no GPU acceleration and constrained RAM) to allow for easy integration into a healthcare setting.

## 5. Conclusions

An open source and free-to-use module was developed that provides bone-thickness and distance-to-first-air cell visualization with submillimeter accuracy for the purpose of aiding in pre-surgical planning. The implemented module was designed to offer advanced configuration options that allow bone-thickness and distance-to-first-air cell visualization on any 3D medical image series. These options allow configuration of critical algorithm parameters such as automation, image segmentation, ray casting, and bone-implant device thickness. As the BONEBRIDGE BCI device was targeted during design and development, specific preset configurations for the BCI-601 and BCI-602 devices were included in the software, however these can be reconfigured to suit any medical device application. This work resulted in a viable surgical planning tool which is intended to reduce pre-surgical planning time and resources. The tool may be utilized as an adjunct to clinical pre-operative planning in multiple disciplines which require the analysis of patient anatomy for bone implants.

## Ethics approval and consent to participate

Approval was obtained from Western University's Committee for Cadaveric Use in Research (Approval number #19062014), and written informed consent was waived.

## Consent for publication

Not Applicable.

## Availability of data and materials

Data associated with this study has been deposited at: https://github.com/Auditory-Biophysics-Lab/Slicer-BoneThicknessMapping.

## Funding

This study was funded by a Collaborative Health Research Projects (CHRP) grant jointly administered by the Natural Sciences and Engineering Research Council of Canada (NSERC) and the Canadian Institutes of Health Research (CIHR). Carlos Daniel Salgado received a scholarship from the National Council of Science and Technology of Mexico (CONACYT). S. Alireza Rohani was funded through a Mitacs Elevate fellowship.

## Authors' contributions

E.S.S, CDS, and SAR developed the algorithm. CDS, HML and SKA conceptualized the project and wrote the manuscript. HML and SKA were primary supervisors for CDS. All authors approved the final manuscript.

## Authors' information

SKA and HML were co-senior authors on this study.

## CRediT authorship contribution statement

**Evan S. Simpson:** Data curation, Formal analysis, Investigation, Methodology, Software, Validation, Visualization, Writing – original draft. **Carlos D. Salgado:** Data curation, Formal analysis, Investigation, Methodology, Software, Validation, Visualization, Writing – original draft, Conceptualization. **Seyed Alireza Rohani:** Data curation, Formal analysis, Investigation, Methodology, Software, Validation, Visualization. **Sumit K. Agrawal:** Conceptualization, Funding acquisition, Project administration, Resources, Supervision, Writing – review & editing. **Hanif M. Ladak:** Conceptualization, Funding acquisition, Project administration, Resources, Supervision, Writing – review & editing.

## Declaration of competing interest

The authors declare that they have no known competing financial interests or personal relationships that could have appeared to influence the work reported in this paper.

## Acknowledgements

Manuscript review provided by Lauren Siegel.

## Abbreviations

BC-FMT – Bone Conduction-Floating mass transducer
CT – Computed Tomography
3D – Three Dimensional
2D – Two Dimensional
BCI – Bone Conduction Implant
HU – Hounsfield units
MAD – Mean Absolute Difference
CI – Confidence Interval

## References

[1] A.M. Huber, J.H. Sim, Y.Z. Xie, M. Chatzimichalis, O. Ullrich, C. Röösli, The Bonebridge: Preclinical evaluation of a new transcutaneously-activated bone anchored hearing device, Hear. Res. 301 (2013) 93–99, https://doi.org/10.1016/j.heares.2013.02.003.
[2] D. Beutner, K.B. Hüttenbrink, Passive and active middle ear implants, GMS Curr. Top. Otorhinolaryngol., Head Neck Surg. 8 (2009) Doc09.
[3] S. Reinfeldt, B. Hakansson, H. Taghavi, M. Eeg-Olofsson, New developments in bone-conduction hearing implants: a review, Med. Devices Evid. Res. 8 (2015) 79–93.
[4] P.A. Dimitriadis, M.R. Farr, A. Allam, J. Ray, Three year experience with the cochlear BAHA attract implant: a systematic review of the literature, BMC Ear Nose Throat Disord. 16 (2016) 1–8.
[5] G.M. Sprinzl, A. Wolf-Magele, The bonebridge bone conduction hearing implant: indication criteria, surgery and a systematic review of the literature, Clin. Otolaryngol. 41 (2) (2016) 131–143.
[6] M.E. Zernotti, A.B. Sarasty, Active bone conduction prosthesis: bonebridge, Int. Arch. Otorhinolaryngol. 19 (4) (2015) 343–348.
[7] Food and Drug Administration, BONEBRIDGE FDA De Novo Summary Documents, 2018. https://www.accessdata.fda.gov/cdrh_docs/pdf17/DEN170009.pdf.
[8] S.K. Plontke, G. Götze, C. Wenzel, T. Rahne, R. Mlynski, Implantation of a new active bone conduction hearing device with optimized geometry. Implantation eines neuen, aktiven, knochenverankerten elektronischen Hörimplantats mit verkleinerter Geometrie, Englische Version HNO 68 (Suppl 2) (2020) 106–115, https://doi.org/10.1007/s00106-020-00877-2.
[9] P. You, L.H. Siegel, Z. Kassam, M. Hebb, L. Parnes, H.M. Ladak, S.K. Agrawal, The middle fossa approach with self-drilling screws: a novel technique for BONEBRIDGE implantation, J Otolaryngol - Head Neck Surg. 48 (2019) 35, https://doi.org/10.1186/s40463-019-0354-7.
[10] L. Siegel, P. You, K. Zimmerman, L. Parnes, S.K. Agrawal, Active transcutaneous bone conduction implant: audiometric outcomes following a novel middle fossa approach with self-drilling screws, Otol. Neurotol. 41 (5) (2020) 605–613.
[11] S.A. Rohani, M.L. Bartling, H.M. Ladak, S.K. Agrawal, The Bonebridge active transcutaneous bone conduction implant: effects of location, lifts and screws on sound transmission, J Otolaryngol - Head Neck Surg. 10 49 (1) (2020) 58.
[12] E.K.C. Law, K.S.S. Bhatia, W.S.S. Tsang, M.C.F. Tong, L. Shi, CT pre-operative planning of a new semi-implantable bone conduction hearing device, Eur. Radiol. 26 (6) (2016) 1686–1695, https://doi.org/10.1007/s00330-015-3983-x.
[13] B.G. Weiss, M. Bertlich, R. Scheele, M. Canis, M. Jakob, J.M. Sohns, Systematic radiographic evaluation of three potential implantation sites for a semi-implantable bone conduction device in 52 patients after previous mastoid surgery, Eur. Arch. Oto-Rhino-Laryngol. 274 (2017) 3001–3009.
[14] E. Vyskocil, D. Riss, C. Arnoldner, J.S. Hamzavi, R. Liepins, A. Kaider, Dura and sinus compression with a transcutaneous bone conduction device – hearing outcomes and safety in 38 patients, Clin. Otolaryngol. 42 (5) (2017) 1033–1038.
[15] G. Sprinzl, T. Lenarz, A. Ernst, et al., First European multicenter results with a new transcutaneous bone conduction hearing implant system: short-term safety and efficacy, Otol. Neurotol. 34 (6) (2013) 1076–1083, https://doi.org/10.1097/MAO.0b013e31828bb541.
[16] T.H. Kong, Y.A. Park, Y.J. Seo, Image-guided implantation of the BONEBRIDGE TM with a surgical navigation: a feasibility study, Int. J. Surg. Case Rep. 30 (2017) 112–117.
[17] S.K. Plontke, F. Radetzki, I. Seiwerth, M. Herzog, S. Brandt, K.-S. Delank, T. Rahne, Individual computer-assisted 3D planning for surgical placement of a new bone conduction hearing device, Otol. Neurotol. 35 (7) (2014) 1251–1257.
[18] W. Wimmer, N. Gerber, J. Guignard, P. Dubach, M. Kompis, S. Weber, M. Caversaccio, Topographic bone thickness maps for BONEBRIDGE implantations, Eur. Arch. Oto-Rhino-Laryngol. 272 (7) (2015) 1651–1658.
[19] M.M. Barakchieva, W. Wimmer, P. Dubach, A.M. Arnold, M. Caversaccio, N. Gerber, Surgical planning tool for bonebridge implantation using topographic bone thickness maps, Int. J. Comput. Assist. Radiol. Surg. 10 (S1) (2015) 97–98.

[20] N. Otsu, A threshold selection method from gray-level histograms, IEEE Trans. Syst. Man. Cybern. 9 (1) (1979) 62–66.
[21] M. Albani, G. Carluccio, P. Pathak, Uniform ray description for the PO scattering by vertices in curved surface with curvilinear edges and relatively general boundary conditions, IEEE Trans. Antenn. Propag. 59 (5) (2011) 1587–1596.
[22] I. Todt, H. Lamecker, H. Ramm, A. Ernst, A computed tomographic data-based vibrant bonebridge visualization tool, Cochlear Implants Int. 15 (Suppl 1) (2014) S72–S74.
[23] H. Ramm, O.S.M. Victoria, I. Todt, H. Schirmacher, A. Ernst, S. Zachow, H. Lamecker, Visual support for positioning hearing implants, CURAC (2013) 116–120.
[24] E.K.C. Law, K.S.S. Bhatia, W.S.S. Tsang, M.C.F. Tong, L. Shi, CT pre-operative planning of a new semi-implantable bone conduction hearing device, Eur. Radiol. 26 (6) (2016) 1686–1695.
[25] N. Matsumoto, J. Hong, M. Hashizume, S. Komune, A minimally invasive registration method using Surface Template-Assisted Marker Positioning (STAMP) for image-guided otologic surgery, Otolaryngol. Head Neck Surg. 140 (1) (2019) 96–102, https://doi.org/10.1016/j.otohns.2008.10.005.
[26] N. Matsumoto, Y. Takumi, B. Cho, K. Mori, S.-I. Usami, M. Yamashita, M. Hashizume, S. Komune, Template-guided implantation of the BONEBRIDGE : clinical experience experience, Eur. Arch. Oto-Rhino-Laryngol. 272 (12) (2015) 3669–3675.
[27] M. Inui, N. Umezu, K. Wakasaki, S. Sato, Thickness and clearance visualization based on distance field of 3D objects, J Comput. Des. Eng. 2 (3) (2015) 183–194.
[28] Thickness Mapping 3D Slicer Module. https://github.com/Auditory-Biophysics-Lab/Slicer-BoneThicknessMapping. Accessed August 1, 2023.
[29] S. Nikan, K. Van Osch, M. Bartling, D.G. Allen, S.A. Rohani, B. Connors, S.K. Agrawal, H.M. Ladak, PWD-3DNet: a deep learning-based fully-automated segmentation of multiple structures on temporal bone CT scans, IEEE Trans. Image Process.: a publication of the IEEE Signal Processing Society 30 (2021) 739–753.